PCCP

Physical Chemistry Chemical Physics

www.rsc.org/pccp

Volume 15 | Number 20 | 28 May 2013 | Pages 7423–7898

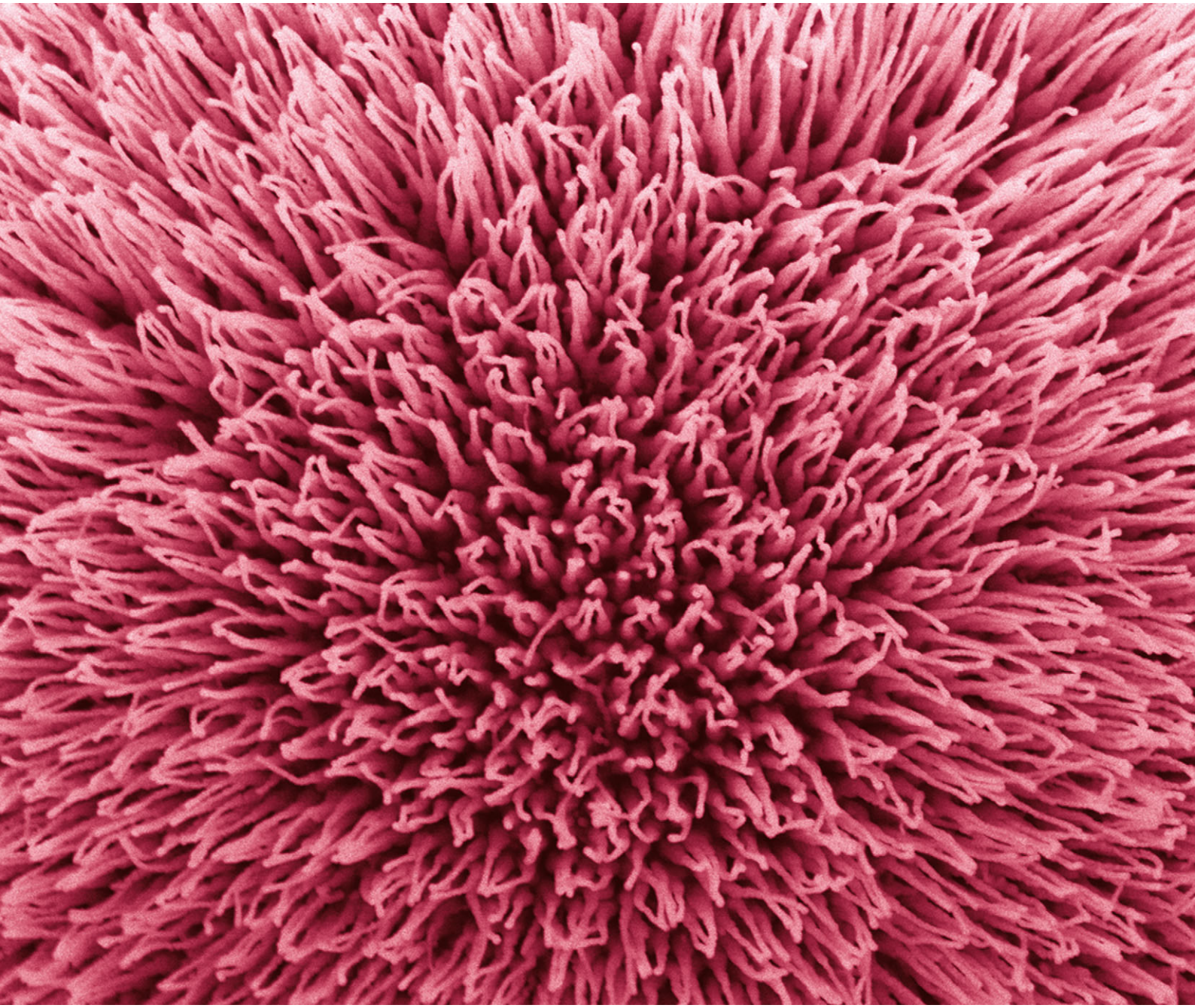

ISSN 1463-9076

PAPER

Zhanjun Gu, Zheng Wei Pan *et al.*

Luminescent Zn_2GeO_4 nanorod arrays and nanowires

1463-9076(2013)15:20;1-S

PCCP

RSC Publishing

PAPER

View Article Online
View Journal | View Issue

Luminescent Zn_2GeO_4 nanorod arrays and nanowires

Cite this: *Phys. Chem. Chem. Phys.*, 2013, **15**, 7488

Zhanjun Gu,*[ab] Feng Liu,[b] Xufan Li[b] and Zheng Wei Pan*[b]

Received 8th November 2012,
Accepted 11th January 2013

DOI: 10.1039/c3cp43977a

www.rsc.org/pccp

Large-area Zn_2GeO_4 nanorod arrays (1.5 × 5 cm) and long Zn_2GeO_4 nanowires (length up to 1 mm) have been controllably prepared at different areas on the substrate using a simple thermal evaporation method. The formation processes for these nanostructures were investigated carefully. The solid state reaction and vapor-solid process have been found to clearly contribute to the creation of the Zn_2GeO_4 nanorod arrays and long Zn_2GeO_4 nanowires, respectively. Photoluminescence (PL) characterization of these nanostructures showed that both the nanorod arrays and nanowires exhibited strong blue-white luminescence. Mn-doped Zn_2GeO_4 nanorod arrays have also been obtained by doping an appropriate amount of Mn^{2+} ions in the products. Zn_2GeO_4 nanostructures doped with Mn^{2+} exhibited bright green luminescence.

Introduction

Light-emitting one-dimensional (1D) nanostructures are of much current interest due to their unique physical properties and their wide-ranging applications in nanoscale light-emitting diodes,[1] photodetectors,[2] lasers,[3] waveguides,[4] and optical switches.[5] For example, lasing in a single CdS nanorod and in ZnO nanowires and nanoribbons were reported by Yang's and Liber's groups, respectively.[3] Tin dioxide (SnO_2) nanoribbons have been shown to act as excellent sub-wavelength waveguides of UV and visible light.[4a] Recently, luminescent nanorod arrays, such as ZnO,[6] ZnS[7] and GaN,[8] have also been realized, which may find realistic applications in light emission and display devices. However, most research into luminescent nanowires is focused on binary compounds such as ZnO, SnO_2, CdS, and GaN. The properties and applications of those nanomaterials are limited due to their simple binary system. In recent years, there has been increasing interest in 1D ternary oxide nanomaterials, such as $ZnGa_2O_4$,[9] Zn_2SiO_4,[10] $MgAl_2O_4$[11] and $ZnAl_2O_4$[12] because of their novel optical properties and potential applications in vacuum fluorescent displays (VFDs), low-voltage field emission displays (FEDs) and electroluminescent displays (ELDs).

Zn_2GeO_4, as a ternary oxide, has been well-known to possess interesting properties that make it a promising candidate for applications in photocatalysis for the decomposition of water,[13] negative thermal expansion material[14] and electroluminescence devices.[15] Very recently, it was reported that Zn_2GeO_4 presented a blue-white emission, and its photoluminescence (PL) was approximately 40% brighter than that of commercial ZnO phosphor.[16] However, the study on nanostructured Zn_2GeO_4 is relatively limited due to the lack of preparation methods for this material. Here, we present a simple strategy to produce luminescent Zn_2GeO_4 nanorod arrays and nanowires by the thermal evaporation of Zn and Ge powder. In this synthesis, large-scale Zn_2GeO_4 nanorod arrays (1.5 × 5 cm) and long Zn_2GeO_4 nanowires (length upto 1 mm) have been controllably prepared at different areas on the substrate. We also discovered that both the nanorod arrays and nanowires showed strong blue-white luminescence. Furthermore, this luminescence can be tuned from blue-white to bright green by doping an appropriate amount of Mn^{2+} into the nanostructure.

Experimental

Materials and substrate

Ge and Zn powders were used as the Ge and Zn sources, respectively. Si wafers were used as the supporting and growth substrates. Ultra high-purity (UHP) oxygen gas was used as the oxygen source and UHP argon was used as the carrier gas.

Growth of nanorod arrays and nanowires

The experiment was conducted in a tube furnace system. In a typical run, about 0.1 g of Ge and 0.1 g of Zn powder were placed at the center of an alumina tube that was inserted in a horizontal tube furnace. Si wafer as the substrate was located about 1 cm downstream from the source materials. After evacuating the alumina tube to $\sim 2 \times 10^{-3}$ Torr, 200 sccm (standard cubic cm min^{-1}) flowing argon was introduced into the reaction chamber and the furnace was heated to 1000 °C (15 °C min^{-1}). About 2 sccm oxygen was added through a long, thin alumina tube to a position right above the growth substrate.

[a] *CAS Key Laboratory for Biomedical Effects of Nanomaterials and Nanosafety, Institute of High Energy Physics, Chinese Academy of Sciences, Beijing, 100049, P. R. China. E-mail: zjgu@ihep.ac.cn*

[b] *Faculty of Engineering, Department of Physics and Astronomy, University of Georgia, Athens, Georgia 30602, USA. E-mail: panz@uga.edu*

At 1000 °C, the Ge and Zn vapor was transported by the argon carrier gas to the growth zone, where the temperature was in the range of 800 to 950 °C, to feed the nanowire/nanorod growth. The pressure of the reaction chamber was held at 300 Torr and the growth time varied from 10 to 30 min. The furnace was then cooled down naturally to room temperature under an Ar flow. Mn doped Zn_2GeO_4 products were simply prepared by adding 0.001–0.0015 g of $MnCl_2$ in the source material while keeping other condition unchanged.

The as-prepared samples were annealed at various atmospheres. N_2, O_2 and air annealing were conducted in a tube furnace. The temperature was maintained at 1000 °C and the flow rates for all gas were kept at 200 sccm. For vacuum annealing, the temperature and the pressure were kept at 1000 °C and 2×10^{-3} Torr, respectively.

Characterization

The as-synthesized products are characterized and analyzed by a X-ray diffractometer (XRD; PANalytical X'Pert PRO diffractometer with Cu Kα radiation), scanning electron microscope (SEM; FEI Inspec F FEG SEM at 15 kV), transmission electron microscope (TEM; Hitachi HF-3300 FEG STEM at 300 kV), and an energy-dispersive X-ray spectroscope (EDS) attached to the SEM and TEM. The photoluminescence (PL) properties were studied with a Horiba Jobin Yvon FluoroLog3-2iHR320 spectrofluorometer using a Xe lamp as the excitation source. The doping concentration of Mn^{2+} in the sample was evaluated by inductively coupled plasma mass spectrometry (ICP-MS, Thermo Elemental X7, USA) analysis. For PL analysis, the sample was excited at 265 nm and the emission spectra were recorded in the range of 350–750 nm at room temperature. For SEM investigation, the products together with the growth substrate were directly transferred into the SEM chamber without destroying the location and orientation of the products on the substrates. For TEM studies, the products were gently scraped off from the substrate using sharp tweezers and were directly mounted onto a Cu folding TEM grid.

Result and discussion

After the reaction, gray and white colored products were obtained on the whole substrate. Scanning electron microscopy (SEM) observation reveals that from the high temperature area to the low temperature area, the morphologies of the products changed gradually with their positions on the Si substrate (Fig. 1). At the low temperature area, as illustrated in Fig. 1a, the surface of the Si substrate (5 × 1.5 cm) was covered by a thin gray layer. Upon irradiation with UV light, a strong photoluminescence was observed from this film (Fig. 1b). This emission appeared as a blue-white color which is usually observed in Zn_2GeO_4 phosphors. SEM observations revealed that this thin film was actually composed of dense, highly-aligned nanorods with a growth direction perpendicular to the substrate surface (Fig. 1c–e). The diameters of these nanorods were about 200–400 nm and the lengths of the nanorods were upto 3–5 um. X-Ray diffraction (XRD) was then used to characterize the structural properties.

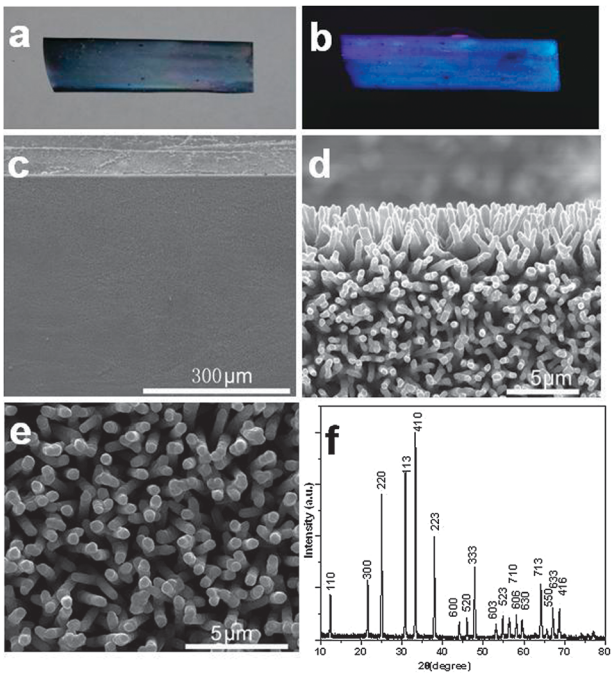

Fig. 1 Vertically-aligned Zn_2GeO_4 nanorod arrays grown on silicon substrate. Optical images of the top view of the substrate with the nanorod arrays grown over the entire surface (a) and (b). A strong blue-white emission is visible with the naked eye upon illumination of the sample with a 254 nm UV lamp. (c) Low-magnification SEM image of Zn_2GeO_4 nanorod arrays, indicating that highly dense and aligned nanorod arrays were grown on a large area. Side (d) and top (e) views of a ZnO nanorod array. XRD pattern (f) of the as-prepared Zn_2GeO_4 nanorod arrays.

As shown in Fig. 1f, all peaks from the products can be well-indexed to rhombohedral Zn_2GeO_4 (JCPDS card No. 11-687). No peaks related to ZnO, GeO_2 or other impurities were detected. More details about the morphological and structural features were obtained from the transmission electron microscopy (TEM) images. The low-resolution TEM image (Fig. 2a) exhibited that the nanorods were straight and the surface was slightly bumpy. The high-resolution TEM image (Fig. 2b) clearly showed that these nanorods are polycrystalline.

Recently, several ZnO-based ternary oxide 1D nanostructures have been reported, such as $ZnGa_2O_4$ nanorod arrays and $ZnAl_2O_4$ nanotubes.[9,12] In those reports, a two-step method was used to synthesize the ternary oxide nanostructures. First, ZnO nanorod arrays were prepared in the first step. Then, these

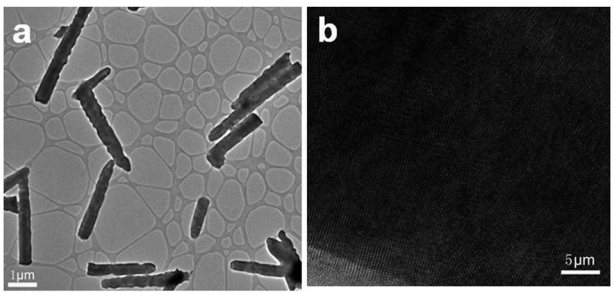

Fig. 2 TEM and high resolution TEM image of the nanorods.

ZnO nanorod arrays were coated with another oxide layer on the surface of the nanorods, which were annealed at high temperature to form the ternary oxides through solid–state reaction. In our experiment, we used a one-step method to synthesize the Zn_2GeO_4 nanorod arrays by direct evaporation of the Zn and Ge powders at 1000 °C. However, in our previous experiment, we also found that ZnO nanorod arrays were easily obtained at low temperature by heating Zn powder at 600 °C due to its low evaporation temperature. This result suggests to us that the ZnO nanorod arrays may be formed first at low temperature and then react with Ge vapor to produce Zn_2GeO_4 nanorod arrays at high temperature. This process is similar to the two-step process for the synthesis of ZnO based ternary oxides proposed in refs. 9,12. To confirm our speculation, we conducted the experiment at different temperatures while keeping other conditions unchanged. When the reaction temperature was conducted at 700 °C, a highly-aligned nanorod array was obtained (Fig. 3a and b). In addition, the surface of these nanorods is smoother compared to that of Zn_2GeO_4 nanorods. The XRD pattern as shown in Fig. 3c clearly shows that these nanorods are in the pure phase of wurtzite ZnO with lattice constants of a = 3.253 Å and c = 5.209 Å (JCPDS card No. 36-1451). Interestingly, a few Ge species were detected by EDS analysis (Fig. 3d). But no germanium or germanium oxide diffraction peaks were found in the XRD pattern, suggesting an amorphous layer of Ge or GeO_2 deposited on the ZnO nanorod. Increasing the temperature to 1000 °C, it can be seen clearly that the morphology of the ZnO nanorod array (Fig. 3e) was retained but that a phase transformation happened during the reaction. After reaction for 10 min, several new peaks indicated by asterisks can be found, which corresponds to the Zn_2GeO_4. Further increasing the reaction time, the intensity of the Zn_2GeO_4 peaks increased distinctly, and the peaks of ZnO gradually dispersed, which suggested that all the ZnO nanorods were transformed to Zn_2GeO_4 (Fig. 3f). Therefore, the growth temperature and the reaction time are critical parameters for the growth of Zn_2GeO_4 nanostructures using ZnO nanorods as templates. The above results clearly show that there are two stages for the formation of Zn_2GeO_4 nanorod arrays. The first stage can be defined as the temperature of the furnace between 450 and 700 °C. This stage lasts about 16 min based on the temperature increasing rate of our furnace (15 °C min^{-1}). In this stage, ZnO nanorod arrays can be easily obtained because zinc has a low evaporation temperature. It is worth noting that we added the oxygen through a long, thin alumina tube to a position right above the growth zone. Adding the oxygen behind the sources plays a key role in the formation of large area ZnO nanorod arrays. The introduction of oxygen downstream from the Zn source can avoid the pre-oxidation of Zn powder, while generating an efficient, wide oxidizing region to facilitate the ZnO nanorod array growth. The detailed formation process of this ZnO nanorod array has been discussed in our previous work and other references.[17,18] The second stage is defined as the temperature of the furnace between 700 and 1000 °C. In this stage, more Ge was evaporated and deposited on the surface of the ZnO nanorod. When the temperature reached 1000 °C, the Ge layer possibly absorbed oxygen from the ambient to form amorphous GeO_2 and then directly reacted with the ZnO nanorod through a solid state reaction, resulting in the formation of Zn_2GeO_4 nanorods. The proposed formation mechanism of the Zn_2GeO_4 nanorod arrays is illustrated in Fig. 3g.

At the high temperature area, the overall morphology of the products was shown in Fig. 4, which showed that the sample was composed of a large quantity of uniform long nanowires with diameters typically in the range of 200–400 nm and length of upto over 1 mm. The aspect ratio of these nanowires is more than 200. Close observation revealed that these nanowires were flexible and had a uniform diameter along their entire length (Fig. 4b). The XRD pattern (Fig. 4c) recorded from the nanowires matched well with that of pure phase of Zn_2GeO_4 (JCPDS card No. 11-687) with lattice constants of a = 14.231 Å and c = 9.530 Å. The peaks were strong and narrow, indicating the good crystallinity of the as-prepared sample. To provide further insight into the composition and structure of the as-prepared nanowires, a few Zn_2GeO_4 nanowires were analyzed by EDS mapping measurement and TEM. EDS mapping results (Fig. 4d and e) revealed that each nanowire was composed of Zn, Ge and O. The atomic ratio of the Zn/Ge/O was about 2 : 1 : 4, which was in good agreement with the XRD result. The TEM image (Fig. 5) showed clear lattice fringes in the nanowire and the regular spacing of the lattice fringes was found to be about 0.716 nm, corresponding to the (110) plane of the Zn_2GeO_4 crystal. This result confirms that the nanowire is a single crystal which grows along the [110] direction.

Apparently, the morphologies of the long nanowires and the Zn_2GeO_4 nanorods are totally different. Thus, the solid state reaction explained how the formation of Zn_2GeO_4 nanorod arrays cannot account for the creation of Zn_2GeO_4 long nanowires. In addition, if the nanowires grew through the solid state reaction, long ZnO nanowires were needed as the template. However, we did not detect the long ZnO nanowires in our experiment. Moreover, the Zn_2GeO_4 nanowire could only be obtained when the furnace reached a high temperature (1000 °C). Through the quartz window located at the right end of the furnace tube, heavy smoke-like vapor was visible during the entire reaction period. Based on these observations, we speculate that the growth mechanism of these nanowires is believed to proceed *via* a vapor-solid growth mechanism which usually explains 1D nanostructure growth in gas phase reactions without catalyst assistance. When the furnace temperature reached 1000 °C (the efficient evaporation temperature for Ge), the Ge and Zn vapors mixed with oxygen and then reacted with each other to form Zn_2GeO_4 nanowires through the vapor solid process. Actually, we observed a similar phenomenon for other material systems, such as the growth of GaP nanowires in our previous report.[19] Due to the gas phases of ZnO and GeO_2 having higher activity than those of the solid phase, the reaction is very quick and efficient, and that is the reason why such long nanowires can be obtained in such a short time (10 min).

Similar to the Zn_2GeO_4 nanorod arrays, these Zn_2GeO_4 nanowires also exhibited a strong blue-white emission.

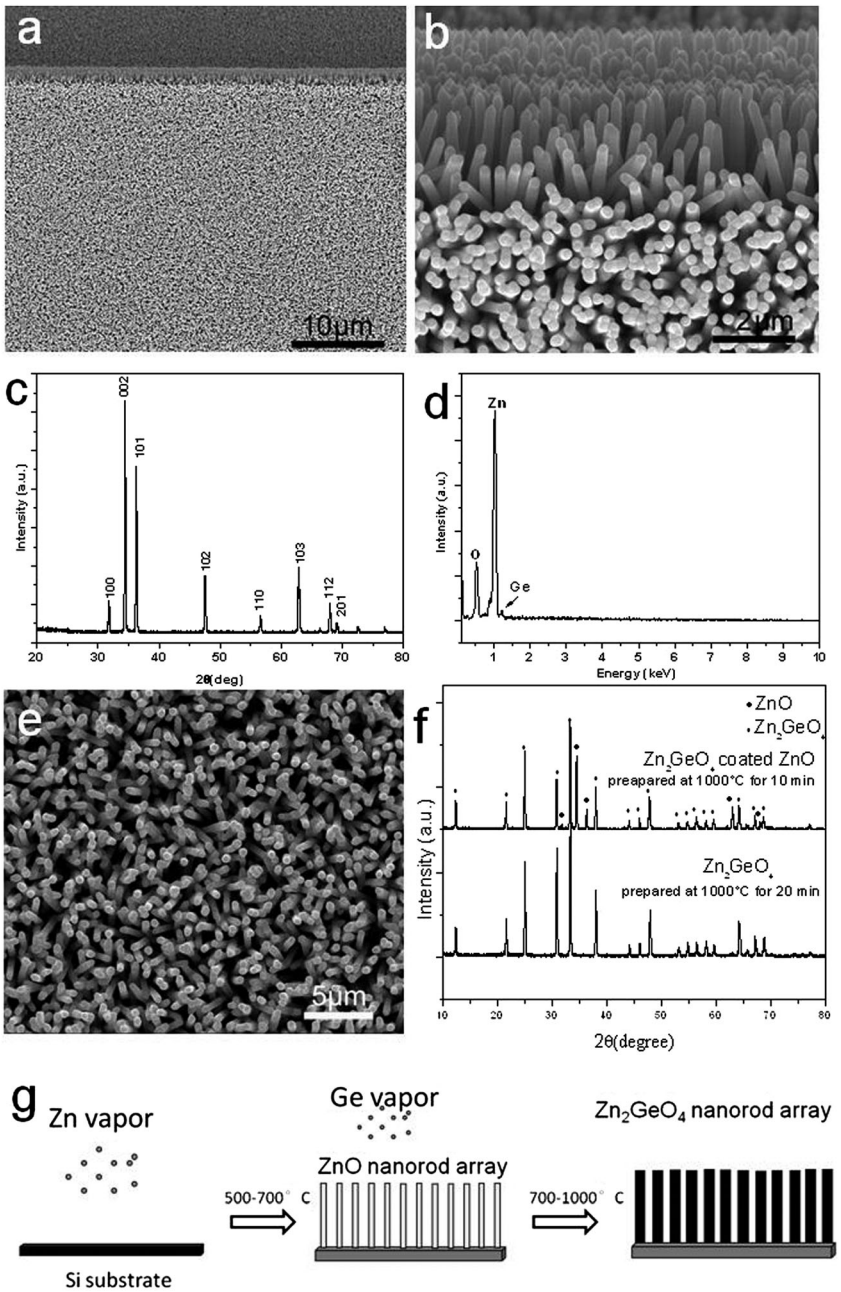

Fig. 3 (a) and (b) SEM image of the nanorod arrays prepared at low temperature (700 °C). (c) XRD pattern of the sample growing at 700 °C. (d) EDS spectrum of the nanorod array recorded from the select area in (a). (e) SEM image of $ZnGe_2O_4$ nanostructures prepared at 1000 °C for 20 min. (f) XRD pattern of sample prepared at 1000 °C for different times. (g) Proposed mechanism for the formation of the Zn_2GeO_4 nanorod arrays.

Fig. 6 showed the florescence microscopy image of the dense growth of long Zn_2GeO_4 nanowires over a large area on the substrate. A bright white-bluish color was visible when the sample was irradiated with 254 nm light from a handheld UV lamp. Interestingly, strong PL emission at the end of the nanowire can be clearly seen in the inset of Fig. 6, while only a weak emission was detected from the side surface of the nanowire, indicating that these nanowires may find applications in waveguide devices.

Room temperature photoluminescence spectra of the long Zn_2GeO_4 nanowires and the Zn_2GeO_4 nanorod arrays are shown in Fig. 7a. Both Zn_2GeO_4 nanowires and Zn_2GeO_4 nanorod arrays showed a broad and strong blue-white emission band ranging from 400–650 nm. The peak positions of these two samples are at 482 nm which is similar with that of Zn_2GeO_4 phosphors reported by previous works.[16,20] Because Zn_2GeO_4 is a kind of self-activated phosphor, its luminescence is contributed to by its native defects, such as oxygen vacancies. To determine the origin of photoluminescence in our sample, we annealed the sample in various atmospheres, such as vacuum, air, N_2 and O_2, in which the O_2 partial pressure was varied. When the samples were annealed at 1000 °C in air and O_2, they no longer exhibited

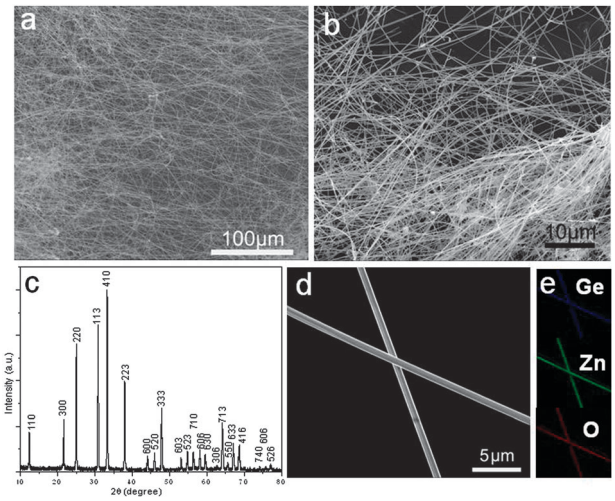

Fig. 4 (a) and (b) SEM image of the long Zn_2GeO_4 nanowires. (c) XRD pattern of Zn_2GeO_4 nanowires. (d) and (e) EDS mapping result of the nanowires.

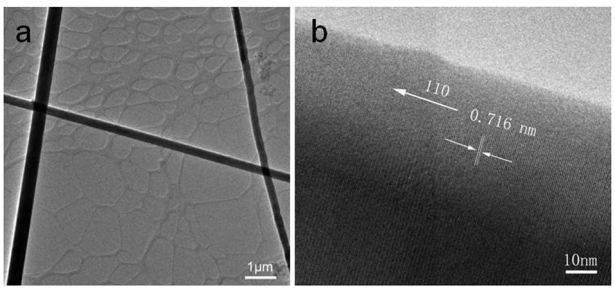

Fig. 5 (a) TEM image of the Zn_2GeO_4 nanowire. (b) High resolution TEM image of the nanowire.

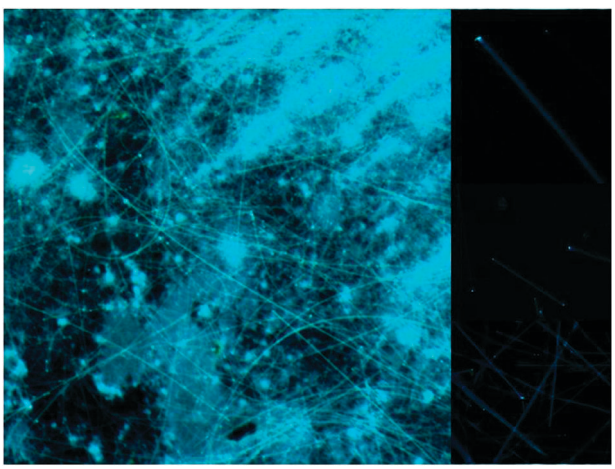

Fig. 6 Florescence microscopy image of the long Zn_2GeO_4 nanowires excited by 254 nm UV light.

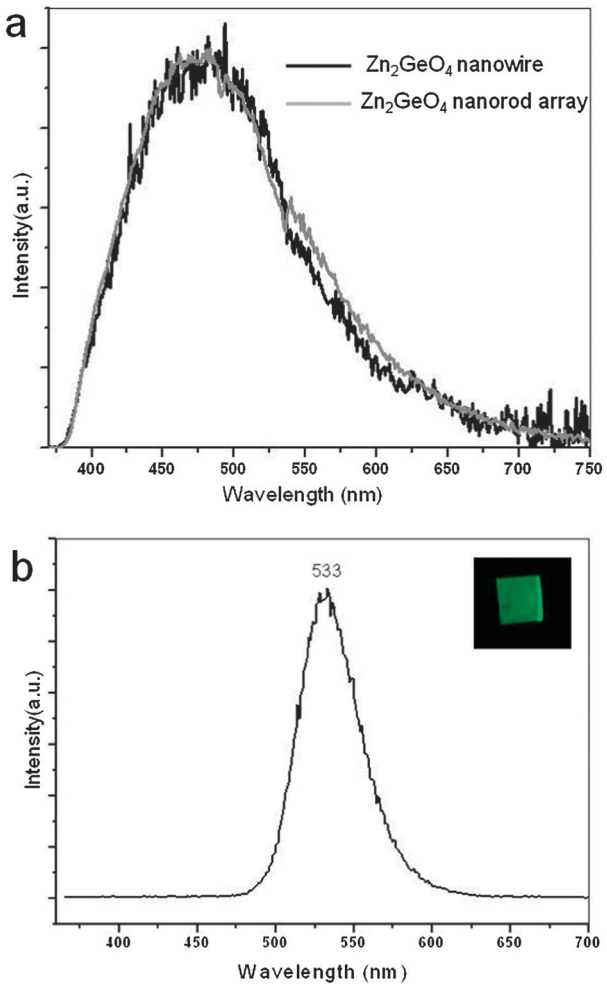

Fig. 7 (a) PL spectra of the as-prepared Zn_2GeO_4 nanostructures at room temperature under excitation at 265nm. (b) PL spectra of the as-prepared Mn^{2+}-doped Zn_2GeO_4 nanorod arrays. Inset in (b) is a digital image of the green luminescent Mn^{2+}-doped Zn_2GeO_4 nanorod arrays.

luminescence, while after annealing in N_2 and vacuum, the luminescent intensity of the samples increased visibly. In N_2 or vacuum atmosphere, the O_2 partial pressure was relatively low, thus the following defect equilibrium (using Kröger–Vink notations[21]) may shift to the right and the density of oxygen vacancies is (V_o^x) increased.

$$O_o^x \rightleftharpoons V_o^x + 1/2O_2 \uparrow$$

When annealing in air or O_2, the O_2 partial pressure was increased and the above equilibrium shifted to the left and the density of V_o^x decreased. Thus, this result clearly shows that the oxygen vacancies play a key role for luminescence in Zn_2GeO_4. Further study is needed for a clearer luminescence mechanism.

Mn-doped Zn_2GeO_4 nanotructures can also be obtained by simply adding an appropriate amount of Mn^{2+} ions to the products. These dopants have no influence on either the morphology or structure of the nanorods. Zn_2GeO_4 doped with Mn^{2+} is well-known to emit green light upon UV excitation. Zn_2GeO_4 has a rhombohedral structure with Zn ions at tetrahedral sites and Ge at octahedral sites. As motioned above, undoped Zn_2GeO_4 is a native defect phosphor and exhibits white-blue luminescence under UV light excitation. After doping Mn^{2+} ions into the Zn_2GeO_4 host matrix, the Mn^{2+} ions

substitute for the tetrahedrally-coordinated Zn^{2+} ions in the host and become the emission centers. Under UV light excitation, the energy transfer from the host to Mn^{2+} then leads to the $^4T_1$-$^6A_1$ transition of Mn^{2+} that exhibits green emission peaked at 533 nm. The results are similar to what has been noted for the green emission from Zn_2GeO_4: Mn phosphors.[22–24] It should also be noted that the doping amount of Mn^{2+} has a strong influence on their luminescence performance. The optimum doping level of Mn^{2+} has been determined to be $x = 0.01$ (x in $Zn_{2-x}GeO_4$: xMn^{2+}) by using ICP-MS analysis. Further increasing the amount of Mn resulted in reducing the emission intensity of the products due to concentration quenching.

Conclusion

In summary, we have successfully grown large area Zn_2GeO_4 nanorod arrays and long Zn_2GeO_4 nanowires on the silicon substrate using a simple thermal evaporation method. The formation mechanisms for these nanostructures have been investigated. The solid state reaction and vapor solid process have been found to clearly contribute to the formation of the Zn_2GeO_4 nanorod arrays and Zn_2GeO_4 nanowires, respectively. These nanostructures give highly blue-white luminescence upon irradiation with a 254 nm UV lamp. Mn-doped Zn_2GeO_4 nanostructures could also be obtained by simply adding an appropriate amount of Mn^{2+} ions to the products. With their specific structures and interesting optical properties, the Zn_2GeO_4 nanorod arrays and long Zn_2GeO_4 nanowires might serve as promising candidates for advanced photonics and optoelectronics.

Acknowledgements

This work was supported by the U.S. National Science Foundation (CAREER DMR-0955908) and the National Basic Research Programs of China (973 program, No. 2012CB932504). TEM characterization was sponsored by Oak Ridge National Laboratory's Shared Research Equipment (ShaRE) User program, which is sponsored by the Division of Scientific User Facilities of BES, U.S. DOE.

References

1 (*a*) X. Duan, Y. Huang, Y. Cui, J. Wang and C. M. Lieber, *Nature*, 2001, **409**, 66; (*b*) Z. Zhong, F. Qian, D. Wang and C. M. Lieber, *Nano Lett.*, 2003, **3**, 343.
2 (*a*) J. Wang, M. S. Gudiksen, X. Duan, Y. Cui and C. M. Lieber, *Science*, 2001, **293**, 1445; (*b*) T. Zhai, Y. Ma, M. Liao, X. Wang, J. Yao, Y. Bando and D. Golberg, *Chem. Soc. Rev.*, 2011, **40**, 2986–3004.
3 (*a*) J. C. Johnson, H. Q. Yan, R. D. Schaller, L. H. Haber, R. J. Saykally and P. D. Yang, *J. Phys. Chem. B*, 2001, **105**, 11387; (*b*) R. Agarwal, C. J. Barrelet and C. M. Lieber, *Nano Lett.*, 2005, **5**, 917.
4 (*a*) M. Law, D. J. Sirbuly, J. C. Johnson, J. Goldberger, R. J. Saykally and P. D. Yang, *Science*, 2004, **305**, 1269; (*b*) D. J. Sirbuly, M. Law, H. Q. Yan and P. D. Yang, *J. Phys. Chem. B*, 2005, **109**, 15190.
5 H. Kind, H. Yan, B. Messer, M. Law and P. D. Yang, *Adv. Mater.*, 2002, **14**, 158.
6 A. Dev, S. Kar, S. Chakrabarti and S. Chaudhuri, *Nanotechnology*, 2006, **17**, 1533.
7 (*a*) S. K. Panda, A. Dev and S. Chaudhuri, *J. Phys. Chem. C*, 2007, **111**, 5039; (*b*) X. Fang, T. Zhai, U. Gautam, L. Li, L. Wu, Y. Bando and D. Golberg, *Prog. Mater. Sci.*, 2011, **56**, 175.
8 T. Wang, F. Ranalli, P. Parbrook, R. Airey, R. Rattlidge and G. Hill, *Appl. Phys. Lett.*, 2005, **86**, 103103.
9 (*a*) K. W. Chang and J. J. Wu, *J. Phys. Chem. B*, 2005, **109**, 13572; (*b*) Y. J. Li, M. Y. Lu, C. W. Wang, K. M. Li and J. Chen, *Appl. Phys. Lett.*, 2006, **88**, 143102.
10 J. Zhou, J. Liu, X. D. Wang, J. H. Song, R. Tummala, N. S. Xu and Z. L. Wang, *Small*, 2007, **3**, 622.
11 H. J. Fan, M. Knez, R. Scholz, K. Nielsch, E. Pippel, D. Hesse, U. Gösele and M. Zacharias, *Nanotechnology*, 2006, **17**, 5157.
12 H. J. Fan, M. Knez, R. Scholz, K. Nielsch, E. Pippel, D. Hesse, M. Zacharias and U. Gösele, *Nat. Mater.*, 2006, **5**, 627.
13 J. Sato, H. Kobayashi, K. Ikarashi, N. Saito, H. Nishiyama and Y. Inoue, *J. Phys. Chem. B*, 2004, **108**, 4369.
14 R. Steven, B. F. Woodfield, J. Boerio-Goates and M. K. Crawford, *J. Chem. Thermodyn.*, 2004, **36**, 349.
15 J. P. Bender, J. F. Wager, J. Kissick, B. L. Clark and D. A. Keszler, *J. Lunin*, 2002, **99**, 311.
16 Z. S. Liu, X. P. Jing and L. X. Wang, *J. Electrochem. Soc.*, 2007, **154**, H500.
17 Z. J. Gu, F. Liu, J. Howe, M. Paranthaman and Z. W. Pan, *ACS Nano*, 2009, **2**, 273.
18 (*a*) G. Z. Shen, Y. Bando and C. J. Lee, *J. Phys. Chem. B*, 2005, **109**, 10578; (*b*) S. Kar, B. N. Pal, S. Chaudhuri and D. Chakravorty, *J. Phys. Chem. B*, 2006, **110**, 4605.
19 Z. Gu, M. Paranthaman and Z. Pan, *Cryst. Growth Des.*, 2009, **9**, 525.
20 M. Y. Tsai, C. Y. Yu, C. C. Wang and T. P. Perng, *Cryst. Growth Des.*, 2008, **8**, 2264.
21 F. A. Kröger and V. J. Vink, *Solid State Phys.*, 1956, **3**, 307.
22 G. B. Che, C. B. Liu, X. Y. Li, Z. L. Xu, Y. Liu and H. Wang, *J. Phys. Chem. Solids*, 2008, **69**, 2091.
23 M. Shang, G. Li, D. Yang, X. Kang, C. Peng and J. Lin, *Dalton Trans.*, 2012, **41**, 8861.
24 S. Takeshita, J. Honda, T. Isobe, T. Sawayama and S. Niikura, *J. Solid State Chem.*, 2012, **189**, 112.